THE JOURNAL OF PHYSICAL CHEMISTRY B

Article

pubs.acs.org/JPCB

Coarse-Grained Molecular Simulation of Self-Assembly for Nonionic Surfactants on Graphene Nanostructures

Dan Wu and Xiaoning Yang*

State Key Laboratory of Materials-Oriented Chemical Engineering, College of Chemistry and Chemical Engineering, Nanjing University of Technology, Nanjing 210009, China

Supporting Information

ABSTRACT: Self-assembly of amphiphilic molecules on the surfaces of nanoscale materials has an important application in a variety of nanotechnology. Here, we report a coarse-grained molecular dynamics simulation on the structure and morphology of the nonionic surfactant, *n*-alkyl poly(ethylene oxide) (PEO), adsorbed on planar graphene nanostructures. The effects of concentration, surfactant structure, and size of graphene sheet are explored. Because of the finite dimension effect, various morphological hemimicelles can be formed on nanoscale graphene surfaces, which is somewhat different from the self-assembly structures on infinite carbon surfaces. The aggregate morphology is highly dependent on the concentration, the chain lengths, and the size of graphene nanosheets. For the nonionic surfactant, the PEO headgroups show strong dispersion interaction with the carbon surface, leading to a side edge adsorption behavior. This simulation provides insight into the supramolecular self-assembly nanostructures and the adsorption mechanism for the nonionic surfactants aggregated on graphene nanostructures, which could be exploited to guide fabrication of graphene-based nanocomposites.

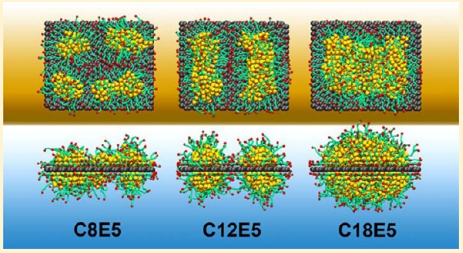

1. INTRODUCTION

Graphene has excellent electronic conductivity, thermal and chemical stability, and mechanical flexibility,[1−3] which can be explored to prepare new-type hybrid nanomaterials with superior properties.[4−7] In this regard, amphiphilic surfactants or polymers are often utilized to direct the preparation of nanomaterials.[8−11] For instance, surfactant self-assembly on graphene surfaces has been used to fabricate well controlled and ordered hybrid metal−oxide/graphene or silica/graphene nanostructures.[12−14] The utilization of surfactant not only solves the hydrophobic/hydrophilic incompatibility problem in nanocomposites but also acts as a molecular template to control the deposition and grafting of functional compounds on nanoscale graphene surfaces.

However, surfactant adsorption on the graphene surface can also assist in the exfoliation and dispersion of graphene nanoparticles in aqueous medium.[15−17] The generated self-assembly aggregate is able to prevent the agglomeration between surfactant-coated graphene sheets[18] and furthermore can be applied to separate single-layer graphene sheets from multilayer ones using the density gradient method.[19]

In general, if amphiphilic molecules are nonionic and biocompatible, they can be extended into living systems for biomedical fields.[20,21] More recently, nonionic poly(ethylene oxide) (PEO)-based surfactants or amphiphilic block copolymers have attracted extensive attention because the PEO segment is biocompatible and holds promise for biomedical purposes.[22,23] Li et al. showed that polyethylene-b-PEO can be periodically decorated along single-walled carbon nanotubes (SWNTs), leading to a unique hybrid structure for a variety of nanoelectronic and biomedical applications.[24] However, it has been reported that the PEO-b-polypropyleneoxide(PPO)-b-PEO triblock copolymer as the structural directing agent yields hemimicelles on graphene surfaces, which can assist the self-assembly of nanostructured silica on the surfaces of the graphene material.[13] In addition, the nonionic PEO-based amphiphilic block copolymers have been successfully applied as dispersing agents to support high graphene concentrations.[25,26]

The adsorption of surfactants on graphene surfaces is a critical step in the above nanotechnologies.[12,13] However, the precise interfacial structure or morphology of surfactants on graphene surfaces has not been unambiguously determined so far. Understanding the self-assembly process and structures, as well as the factors affecting the aggregate morphology, will guide an improvement in the graphene dispersion and facilitate the design of novel graphene-based nanomaterials.[13,27] Present experiments hardly probe the microscopic structure in the interfacial region of micelles aggregated on solid surfaces. Although there are considerable experimental studies regarding surfactant adsorption on macroscopic surfaces,[28−32] the surfactant self-assembly structures on nanosized surfaces remain unresolved. As pointed by Schartz,[33] experimentally manipulating the objects on a nanoscale is often fraught with difficulty.

Molecular dynamics (MD) simulation is a useful tool to provide molecular insight into the process and structures for surfactant self-assembly on nanoparticle surfaces.[34,35] Although

Received: May 7, 2012
Revised: July 1, 2012
Published: August 9, 2012

dx.doi.org/10.1021/jp3043939 | J. Phys. Chem. B 2012, 116, 12048−12056

atomistic MD simulations with limited time-scale have been reported on the aggregated structures for ionic surfactants on graphene sheets,[35,36] longer time-scale beyond the routinely accessible regime via atomistic simulation is highly preferable. Although self-organization of the nonionic *n*-alkyl PEO surfactants on a planar graphite-like model surface has been simulated using a coarse-grained (CG) simulation in the work of Srinivas et al.,[37] they did not consider the real graphene solid surface with nanoscale. To our best knowledge, aggregated structures of the PEO-based nonionic surfactants absorbed on nanoscale graphene surfaces have not been reported. On account of the finite surface size effect,[35] it is speculated that unique self-assembly structure and adsorption mechanism could be observed for surfactants adsorbed on the nanoscale graphene surfaces, which will be different from the observation in infinite graphite surfaces.

In the present study, the aggregated structures and morphologies of the nonionic surfactants, *n*-alkyl PEO, (C*m*E*n*) on nanosized graphene sheets were simulated using a coarse-grained MD simulation. This type of nonionic surfactant has a nonpolar hydrocarbon tail group (C*m*) and a polar nonionic PEO headgroup (E*n*). We used the MARTINI 2.0 force field throughout the simulation,[38−40] where three or four heavy atoms are approximately modeled as a CG particle. This simulation may lead to a considerable increase in the ability to access the larger space- and time-scales.[39,41] Therefore, it can capture more actual structure and process. The effects of the packing density, the alkyl chain length (*m*), the length of PEO segment (*n*), and the graphene surface size have been investigated. This simulation result can offer a direct microscopic picture or view of the supramolecular surfactant/graphene nanostructures.

2. SIMULATION METHODS

In this work, all coarse-grained simulations were performed using the Lammps package.[42] The MARTINI force field was used throughout the simulation.[40,43] The mapping of atomistic C*m*E*n* into CG beads is typically depicted in Figure 1, where we took penta(oxyethylene)-*n*-dodecyl ether (C12E5) as an illustration. The CG hydrophobic tails are mapped by two C1-type beads and one C2-type bead. Particle types C1 and C2 stand for butane- and propane-type hydrocarbon analogues, respectively. The hydrophilic heads were represented by the SN0-type (C−O−C, methyl ether) bead and the SP2-type (C−OH, methanol) bead. The resultant CG model (C12E5) can be represented by 9 connected beads. In the CG graphite and graphene model, we used a 4:1 mapping of the graphene/graphite carbon atoms, modeled as a C1-type bead (Figure 1), in order to preserve their hexagonal symmetry, as previously reported by Wallace and Sansom.[39,44,45] Similarly, standard CG water is united into a single P4-type bead, mapped from 4 atomistic water molecules in a constant dielectric medium. In order to prevent artificial freezing of CG water, 10% of the total normal water particles are modeled with the antifreeze CG water.[40]

In the simulation of C*m*E*n* at the graphite−water interface, we considered the surfactants C12E3 and C12E5. The graphite structure consists of three graphene layers with AB stacking, which was modeled as the infinite rigid slab in the *xy*-plane, and the periodic boundary condition was used along the *x*- and *y*-directions. Sufficient CG water particles were then inserted into the simulation box to reach the desired density (~1 g/cm^3).

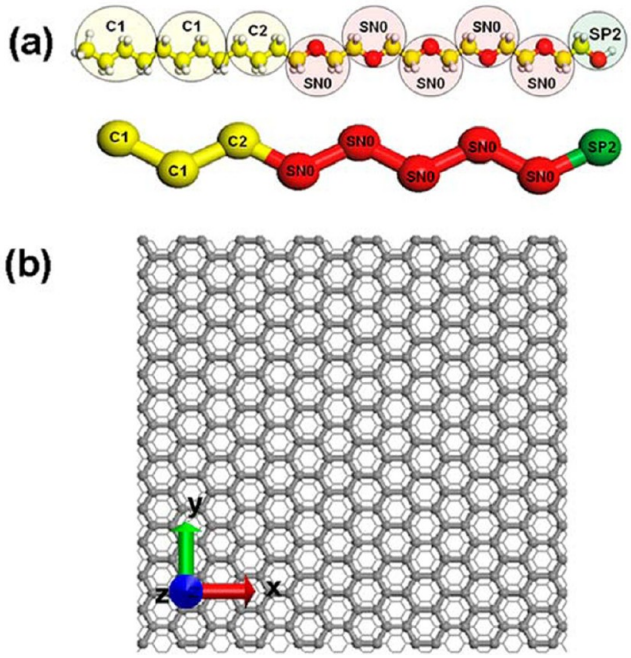

Figure 1. Coarse-grain mapping of an all-atom (AA) C12E5 surfactant molecule (a) and a SWNT structure (b). The hydrophobic (C12) tails are represented by coarse-grain units C1 and C2. C1: nonpolar bead with 4:1 mapping of C atoms. C2: nonpolar bead with 3:1 mapping of C atoms. The hydrophilic heads represented by coarse-grain units SN0 and SP2. SNO: headgroup particle mapping of C−O−C atoms. SP2: headgroup particle mapping of C−O−H atoms.

Simulations were performed in the NVT ensemble at 298.15 K for at least 400 ns. A time step of 10 fs was used.

For the self-assembly simulation of C12E5 on the graphene sheet, the rigid graphene was selected throughout this simulation because there is no obvious difference in the simulation structures between rigid and flexible graphenes, as observed in previous studies.[35,41] The graphene was fixed in the center of simulation box. Sufficient CG water particles were inserted in order to reach the desired density (~1 g/cm^3) within the simulation cell. The simulations were performed in the NPT ensemble at T = 298.15 K, P = 1.0 bar with periodic boundary conditions along three directions. Each system was carried out at least for 480 ns. The time step for integrating Newton's equations is 8 fs. The coordinates were saved every 80 ps for analysis. All the simulation systems are listed in Table S1 in the Supporting Information.

3. RESULTS AND DISCUSSION

In order to verify the rationality of the used Martini force field, we first simulated the self-assembly morphology of the C12E2 surfactant in bulk aqueous phase at 298 K. A well organized lamellar phase is formed with 66 wt % C12E2 solution, as shown in Figure 2a. The obtained lamellar structure is in line with the previous X-ray diffraction study on the C12E2/water system.[46] The corresponding lamellar spacing in our simulation is 4.71 nm, which is in good agreement with the available experimental value (4.73 nm).[46] Meanwhile, our simulation result for the bulk C12E2/water system based on the MARTINI force field agrees well with the previous simulation using a different CG model.[47] We also simulated the bulk phase behavior of the C12E6/water system under two different compositions, 13 wt % and 80 wt % of C12E6 surfactants,

dx.doi.org/10.1021/jp3043939 | J. Phys. Chem. B 2012, 116, 12048−12056

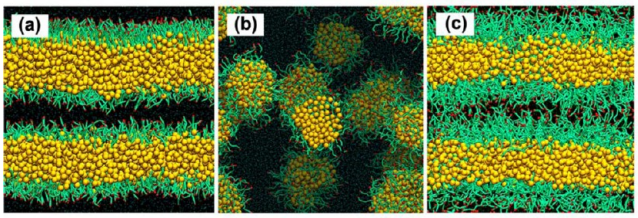

Figure 2. Final equilibrium snapshots from the CG simulations of (a) 66 wt %, (b) 13 wt %, and (c) 80 wt % of C12E6 surfactant solution. Surfactant tailgroups and the end of headgroups are shown by ball representation, while the rest of the headgroups are represented by a stick representation. Color code: yellow, C1 and C2; green, SN0; red, SP2.

respectively, at 298 K. In the case of 13 wt %, the C12E6 surfactants spontaneously form into spherical micelles in the aqueous phase, as seen in Figure 2b. For the concentration of 80%, surfactants organize into the lamellar formation (Figure 2c). The simulated self-assembly structure shows good agreement with the experimental phase diagram of the C12E6/water system.[48] Our simulation results reveal that the MARTINI force field is capable of capturing the important self-assembly structures and behavior of the C*m*E*n* surfactants in bulk aqueous phase.

It should be noted that the MARTINT force field has been parametrized for the fluid phase. Properties of solid/liquid interface are not expected to be very reliable. Therefore, in our systems, the interaction parameters between surfactants and solid surfaces should be used with care. To evaluate the reliability of the CG model in describing the interfacial behavior of the alkyl PEO surfactants on carbon surfaces, we simulated the self-assembly structures of the C*m*E*n* surfactants adsorbed on macroscopic graphite surfaces and compared the simulation results with available experimental results. Herein, in order to reproduce the experimentally observed self-assembly structures and morphologies,[28] the interaction between the surface and the surfactant has been adjusted, that is, the interaction strength (ε) between the CG tailgroups and the CG carbon particles in the graphite was reduced to 60% relative to the original MARTINI parameter value.[40] This parametrizing approach has been adopted in previous CG simulations of lipids on carbon nanotubes.[39,45] We simulated two types of surfactants on graphite surfaces, i.e., C12E3 and C12E5. For C12E3, the aggregates form a bilayer coating on the graphite surface, as displayed in Figure 3a. However, the C12E5 surfactants assemble into continuous hemicylinders on the graphite surface, and the stripe spacing, corresponding to the center-to-center distance between neighboring hemicylindrical micelles, is approximately 5.2 nm (Figure 3b). The simulated self-assembly structures on the graphite surface are consistent with the experimental results reported by Patrick et al.,[28] who showed that the C12E3 surfactants form bilayers on graphite and the C12E5 surfactants are capable of assembling into straight and regular stripes with periodicity of approximately ~5.6 ± 0.2 nm at the graphite−water interface. Srinivas et al.[37] have developed a CG model for the alkyl PEO surfactants and simulated the self-assembly of the surfactants on a graphite-like model surface using the CG model, which is different from the MARTINI force field used in this work. They concluded that the C10E3 surfactants with a short chain can shape into a bilayer structure and the longer-tail C12E5 surfactants can form continuous hemicylinders with diameter ~5.0 ± 0.5 nm. Their

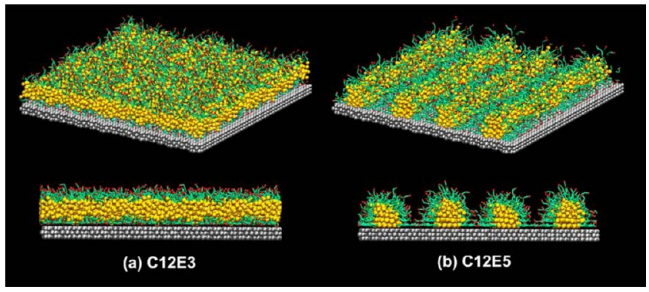

Figure 3. Adsorption morphologies of C12E3 (left panel) and C12E5 (right panel) surfactants on graphite surfaces as observed in the CG simulations. Water molecules are not shown for clarity. The graphite is shown in the gray ball form. Color scheme and other details are the same as that in Figure 2. For visualization, the aggregate structure is replicated along the *x*- and *y*-directions.

simulation result[37] is in good agreement with that obtained in our simulation.

It should be noted that a disordered aggregate structure, rather than the hemicylindrical micelles, is observed for C12E5 on graphite surfaces, if using the original MARTINI force field parameters. The above simulation results show that this reasonable parametrization of MARTINI force field is able to properly describe the self-assembly structures and morphologies for the C*m*E*n* surfactants adsorbed on carbon surfaces.

3.1. Dynamic Process of Surface Adsorption and Self-Assembly. In the surfactant-based stabilization of nanoparticles, the solution usually requires sonication, leading to a random distribution of surfactant molecules. Thus, it is very interesting to learn the adsorption and self-assembly process for the nonionic surfactants on the nanosized graphene surfaces. Therefore, we investigated the dynamic process of C12E5 self-assembly on graphene. The representative snapshots of the process were presented in Figure 4a (see the movie in the Supporting Information), where the surface adsorption area is 0.6 nm^2/molecule at final equilibrium.

During the initial stage, the scattered surfactants begin adsorbing onto the graphene surface and lay horizontally on the surface with their headgroups orienting toward the graphene edge. In order to quantitatively describe the dynamics of adsorption, we used a so-called moment of inertia *M*, which is defined as the total sum of mass of each particle in a chain times the square of their perpendicular distance relative to the surface of graphene, depicted by the following equation:

$$M = \sum_{i=1}^{n} m_i r_i^2 \quad (1)$$

where *i* is the particle number, m_i is the mass of the *i*th particle, and r_i is the vertical distance of the particle relative to the surface. The degree of adsorption and self-assembly can be characterized by a change of *M* as a function of simulation time (see Figure 4c). The *M* value is stable after 400 ns, indicating that the system is well equilibrated. A significant drop in the *M* value at the initial stage (0−33 ns) corresponds to an initial fast adsorption because the carbon surface is uncoated. At the same time, the surfactants also spontaneously self-assemble in the bulk phase.

In addition, the time evolution of the interaction energies between selected groups, including the surface-head (E_{sh}), the water-head (E_{wh}), the surface-tail (E_{st}), and the water-tail (E_{wt}), was shown in Figure 4d. At the beginning, an obvious decrease

dx.doi.org/10.1021/jp3043939 | J. Phys. Chem. B 2012, 116, 12048−12056

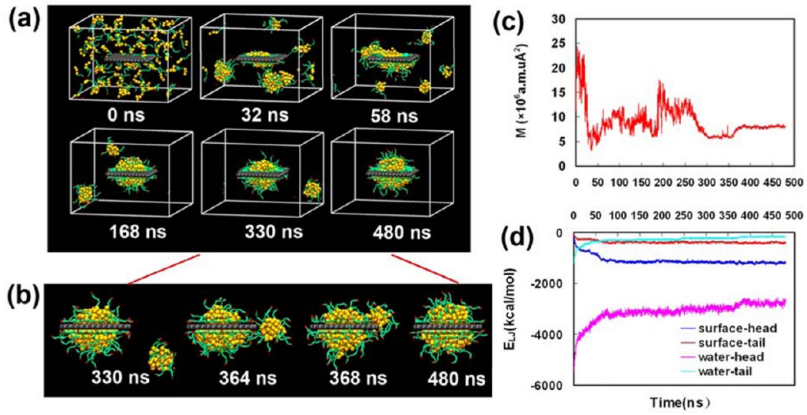

Figure 4. (a) Snapshots of C12E5 surfactants adsorbed onto the graphene surfaces from bulk solution. Water molecules are not shown for clarity. The graphene is shown in the gray ball form. Color scheme and other details are the same as that in Figure 2. (b) Snapshots of C12E5 side absorption process. (c) Change of the inertia moment M as a function of simulation time. (d) Time evolution of the interaction energies of the surface-head (E_{sh}), the water-head (E_{wh}), the surface-tail (E_{st}), and the water-tail (E_{wt}).

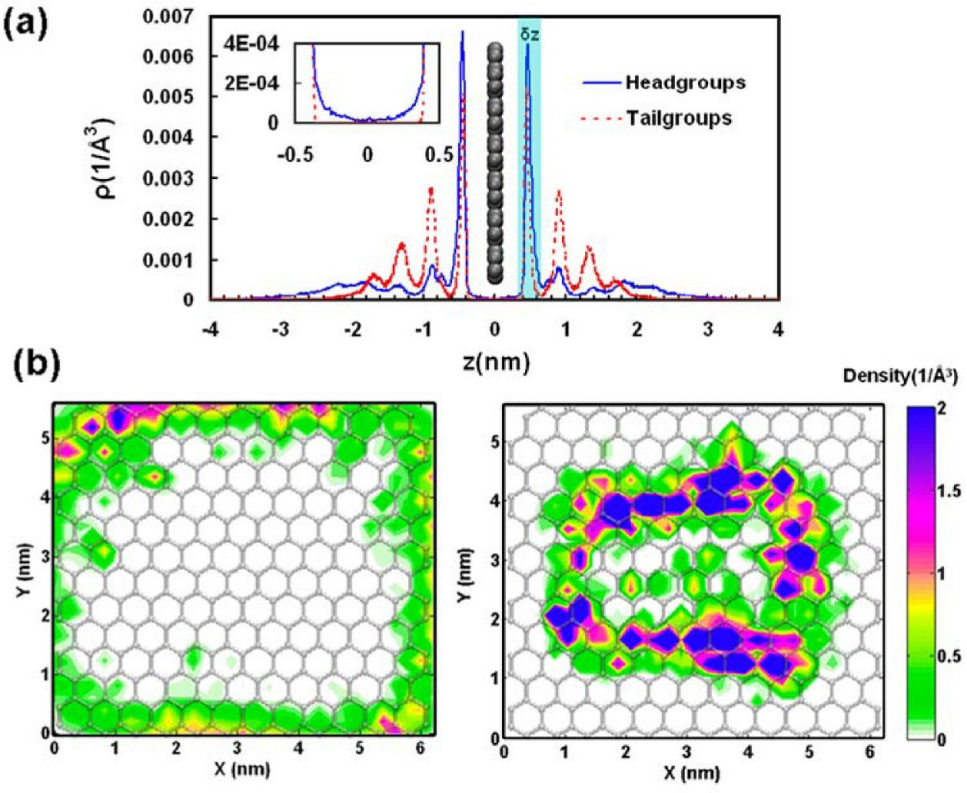

Figure 5. (a) Density profiles for surfactant tailgroups (red line) and headgroups (blue line) in the direction perpendicular to the graphene plane. (b) Surface density distributions of headgroups and tailgroups on graphene for the contact layer that corresponds to the first peak in the density profile, as illustrated by the light blue region in panel a.

in E_{sh} and E_{st} is consistent with the fast adsorption toward the surface, whereas an increase in E_{wh} and E_{wt} is generally related to the concurrent self-assembly process in bulk phase. After the simulation time of 50 ns, the inertia moment M appears to have an evident fluctuation, which is possibly due to two occurring processes: (1) the adsorbed surfactants start to reorganize themselves on the solid surfaces and (2) small micelles in bulk phase fuse with each other and further become larger micelles.

Interestingly, after 300 ns, there appears a steady and lower value of M, which corresponds to the contact of the suspended micelle in the bulk phase with the side edge of graphene. This is because at this stage, the uncoated side edge of graphene provides more chance to attract the surfactants. Once the free micelle contacts with the graphene edge, as shown in Figure 4b, the headgroups in the free micelle first interact with the graphene edge, and then the surfactant molecules within the micelle adjust their packing pattern to combine with the surfactants already adsorbed on the graphene surface. This behavior is different from the feeding adsorption mechanism on infinite graphite proposed in the work of Srinivas et al.[37] A rise after 360 ns in the inertia moment curve (Figure 4c) and in the energy curves of E_{wh} and E_{wt} (Figure 4d) corresponds to the

dx.doi.org/10.1021/jp3043939 | J. Phys. Chem. B 2012, 116, 12048−12056

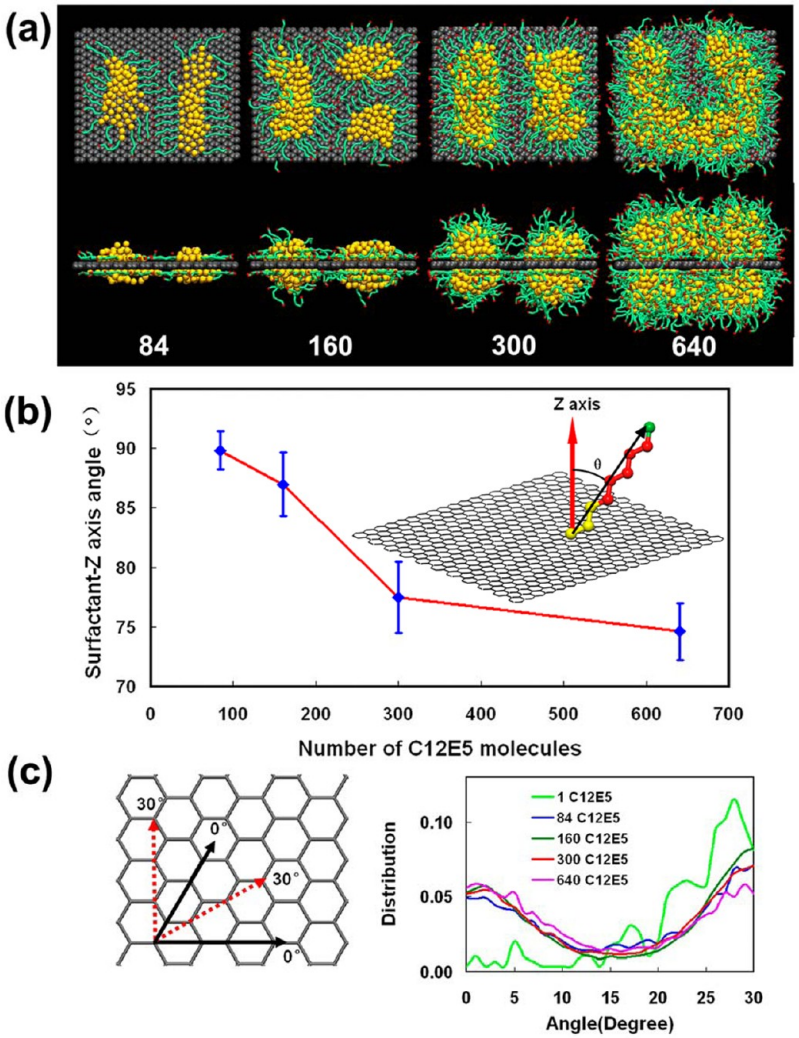

Figure 6. (a) Snapshots of equilibrium morphologies of the C12E5 surfactants with varying concentration on the graphene. Two views for each system: top is a front view, bottom is a side view. Color scheme and other details are the same as that in Figure 4. (b) Orientation angle θ relative to the surface normal as a function of surfactant concentration. (c) Surface orientation distribution of hydrocarbon backbone in the surfactant relative to the plane axes.

process of side edge adsorption. In addition, we have made supplementary simulation for the dynamic processes of 300 C12E5 self-assembly on different graphene nanosheet. Similar dynamical simulation mechanism can be observed (see Figure S2 of the Supporting Information). In short, our simulation presents a clear visual analysis for the adsorption and self-assembly dynamic process.

3.2. Interfacial Self-Assembly Structures. In Figure 4a, the final self-organization of C12E5 on the graphene nanosheet shows a hemisphere configuration with the headgroups orienting radiantly toward both the graphene edge and the water phase. Because of the finite size of the graphene sheet, no hemicylinder aggregate was formed. This kind of surfactant arrangement tends to minimize the contact between the hydrophobic carbon surface (or tailgroups) and the aqueous environment. It is observed that the generated hemispherical micelle does not show stacked layers parallel to the graphene surface, as observed for sodium dodecyl sulfate (SDS).[35] This distinction is likely caused by the different headgroups between the nonionic and the ionic surfactants.

In order to further quantify the interfacial structure features, the density profiles of the tailgroups and headgroups for the C12E5 surfactant are shown in Figure 5a, as a function of the distance z perpendicular to the graphene surface. In the density distribution, the origin on the z-axis corresponds to the location of the graphene surface. The tailgroup (headgroup) density profile was calculated by considering the position of each C1 or C2 (SN0 or SP2) bead of the surfactant backbone. In the tailgroup density profile, the first sharp peak (Figure 5a) indicates that the tail segments present a pronounced adsorption layer near the graphene surface. The first sharp peak in the headgroup density distribution locates at the same position as tailgroups. This suggests that the surfactant molecules in the first adsorption layer prefer to be parallel to the plane. The height of the density peaks decreases as the distance increases, which is consistent with the hemispherical aggregates. The insert of Figure 5a shows a zoomed-in visual of the density profiles very close to the surface. It is noteworthy that the density of headgroups around the graphene sheet does not decay to zero, reflecting a strong side edge effect that keeps the end of headgroups clinging to the graphene edge.

To probe the packing performance of the C12E5 surfactants in the contact adsorption layer, we calculated the two-dimensional surface density distributions for the headgroups

dx.doi.org/10.1021/jp3043939 | J. Phys. Chem. B 2012, 116, 12048−12056

and tailgroups (see Figure 5b). We considered a thin slab whose location corresponds to the first peaks in the density profiles with the thickness (δz) of 0.3 nm, as illustrated in Figure 5a. It is observed that the headgroups arrange themselves at the edge section of the graphene surface, in accordance with the aforementioned density profiles of headgroups. This lateral adsorption can maximize the contact of headgroups with the water surrounding, which is similar to the behavior that the headgroups of SDS molecules are always next to the rising edges of graphite steps.[49] However, this edge adsorption behavior reflects that, despite the hydrophilic nature of PEO segments, the carbon surface has shown a strong dispersion interaction with the headgroups, which has been reported in the previous simulation[50] of PEO brushes grafting on graphite surface in aqueous solution.

3.3. Self-Assembly Morphologies As a Function of Surfactant Concentration. In Figure 6, we show the self-assembly behavior under various concentrations of the C12E5 surfactant. Representative snapshots (Figure 6a) show that a change in surface coverage can generate different aggregate structures. The adsorption of 84 surfactants yields an adsorption surface area of 1.9 nm^2 per molecule, which is obviously lower than the saturation adsorption of the nonionic surfactants on silicon surface (0.52 nm^2 per molecule).[51] In the case of low surface coverage, the graphene is only decorated by monolayer surfactants, which are in parallel attached to the surface with the tail-to-tail and head-to-head arrangements. We found that the hydrophobic tails are completely exposed to the aqueous solution, indicating that, in this low coverage, the headgroups always try to shield the hydrophobic carbon surface rather than the hydrophobic tails. This self-assembly aggregate is consistent with the adsorption pattern of the nonionic surfactant on the graphite surface under low concentration, where a horizontal surface monolayer with surfactant molecules arranged tail-to-tail and head-to-head along one of the graphite symmetry axes.[28] With an increase in the concentration of surfactants (160 surfactants), there is formation of polymorphic aggregate structures, including hemispheres and hemicylinders. These diverse morphologies symbolize a competitive effect between surfactant−surfactant interaction and surfactant−surface interaction. This self-assembly performance not only enhances the isolation of the hydrophobic graphene surface from the surrounding water environment but also maximizes the interacting degree between surfactants.

With 300 surfactants, the adsorption surface area per surfactant is approximately 0.53 nm^2/molecule. We observed that the surfactants form two hemicylinder structures on the each surface of graphene with a spacing of ~5.0 nm along the zigzag axes of the graphene plane. This spacing width is close to the hemicylinder spacing on infinite graphite surface (Figure 3). Under this relatively high coverage, the hydrophobic tails of adsorbed surfactants prefer to aggregate together rather than spread over the entire available surface. This self-assembly manner can keep most of the tailgroups and graphene surface away from water, which is consistent with the experimental AFM data[28,32] for the self-organization of C12E5 on graphite. Meanwhile, it is still observed that a portion of surfactants is parallel to graphene surface with their ends of headgroups toward the water phase on the outer edge of graphene.

In the case of 640 surfactants, two U-shaped micelles are separately located on the top and the bottom of graphene. This unique morphology is different from previously reported structures for surfactants adsorbed on graphite. Once bound to the aggregate structure, the nonionic surfactants do not leave the aggregate during the simulation time. We further conducted a simulation with 792 surfactants absorbed on graphene (0.20 nm^2/molecule). A bulky connected micelle was formed with the graphene sheet packed in the micelle center (see the snapshot of Figure S1, Supporting Information). This is similar to an experimental observation[52] on the formation of large micelles in bulk aqueous phase, where carbon nanotubes were completely wrapped up inside the micelles.

We calculated the orientation distribution of the C12E5 molecules with respect to the graphene plane (Figure 6b). The orientation angle θ is defined as the angle between the normal vector and the vector from the center of mass of the tailgroups to the end of the C12E5 head particle (see the illustration in Figure 6b). In general, a small orientation angle signifies that the surfactants are approximately perpendicular to the graphene surface. As seen in Figure 6b, the orientation angle decreases with an increase in the coverage, consistent with the configuration snapshots in Figure 6a. In particular, at the lowest surfactant concentration, the orientation angle is near 90°, showing a nearly parallel monolayer adsorption arrangement (see Figure 6a).

As discussed earlier, the adsorbed C12E5 molecules within the contact layer near the graphene surface prefer a parallel packing arrangement. It is very interesting to understand the orientation of the surfactant backbone with respect to the zigzag (30°) or armchair (0°) axes of the graphene plane. We analyzed the adsorbed surfactants only within the monolayer near graphene surface at different surface coverages. Figure 6c presents the orientation distributions of the angles between the graphene axes and the vector C1−C2 in the hydrocarbon backbone (C1 and C2 denote the two extreme CG particles in the hydrocarbon backbone of surfactant). An isolated C12E5 exhibits a large tendency to orient along the zigzag (30°) axes, similar to SDS and dodecane.[53] This behavior has been ascribed to the possible match between the hydrocarbon tailgroups and the graphene carbon atoms. However, the filled C12E5 molecules exhibit two distinct tendencies to orient along both the armchair and the zigzag axes, respectively. Comparably, the orientation tendency along the zigzag axes is relatively larger. This preferential orientation is probably due to the specific surface affinity of the long hydrophilic headgroups in the nonionic surfactants.[50]

In the present work, we only simulated the morphologies of the nonionic C*m*E*n* surfactant on the smooth graphene surface. Actually, the topology of surface may affect the micellar morphology of adsorbed surfactants.[54] However, a tentative simulation shows that, for the present nonionic surfactants, the small roughness on the carbon surface may have a weak effect on the self-assembly morphology of surfactants (data not shown). The possible reason is that our nonionic surfactant has a longer headgroups, which could eliminate the effect of surface roughness. However, further detailed research is necessary, which will be carried out in the future work.

3.4. Self-Assembly Morphologies As a Function of Chain Length. In the following section, we simulated the self-assembly structures of the nonionic surfactant with varying lengths of the hydrophilic and hydrophobic domains. We first compared the morphologies of C8E5, C12E5, and C18E5 surfactants with different tail lengths. For each surfactant, the same surface coverage (300 surfactants) was considered, which corresponds to the adsorption surface area of 0.53 nm^2/molecule. As shown in Figure 7, for the short tail surfactant

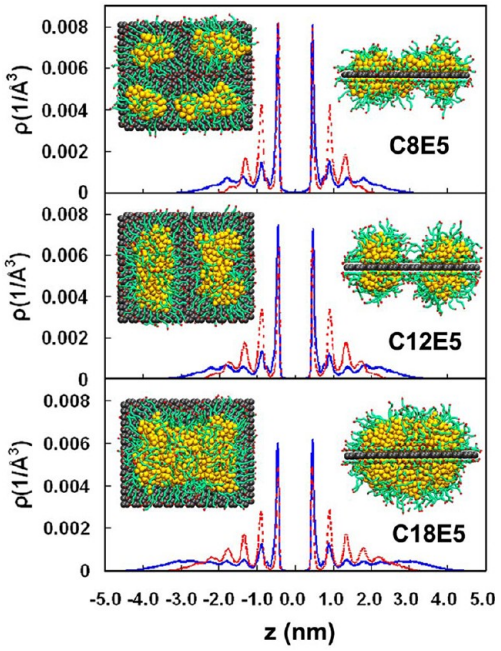

Figure 7. Snapshots of equilibrium morphologies and density profiles of the surfactants with different tail lengths on the graphene. Notice the two views for each system: left is a front view; right is a side view. All water molecules are removed for clarity; color scheme and other details are the same as that in Figure 4.

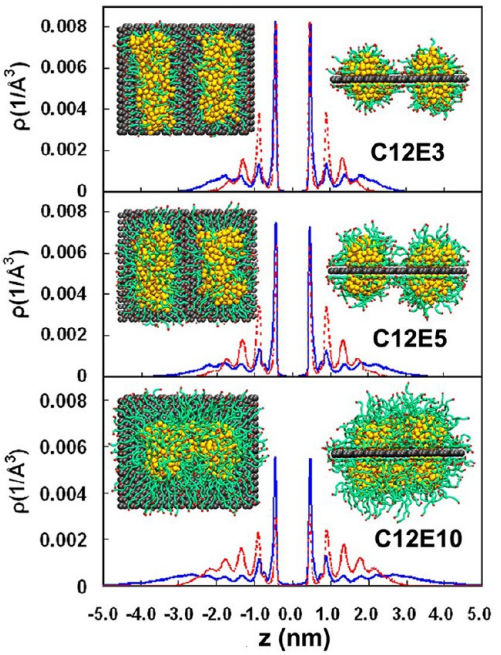

Figure 8. Snapshots of equilibrium morphologies and density profiles of the surfactants with different head lengths on the graphene. Notice the two views for each system: left is a front view; right is a side view. All water molecules are removed for clarity; color scheme and other details are the same as that in Figure 4.

(C8E5), hemispherical micelles appear on the graphene surface. This agrees with the simulated adsorption morphology for a model surfactant with a short tail on the carbon nanotube surface.[55] Previous studies[32,56] have demonstrated the effect of the length of an alkyl chain in nonionic surfactants on the adsorption structure and indicated that the alkyl PEO surfactant with short tails below a critical length is not able to form hemicylindrical micelles on graphite surfaces.

With the length of tailgroups increasing, the hemicylindrical aggregate starts to emerge, and the radius of hemicylindrical micelles (average distance from the solid surface to the end of headgroups in the *z*-direction) increases. This kind of hemicylinder structure is somewhat similar to the striation patterns experimentally observed on the solid surface.[28,32] Meanwhile, this result shows that the volume of hemicylindrical micelles increases with the length of surfactants, indicating that a longer tail produces a larger spatial volume of the self-assembly structures. This can probably be utilized to tailor the supramolecular self-assembly morphologies on nanosized graphenes and to regulate the layer thickness in a sandwiched nanocomposite structure.[12,13]

The relevant density profiles were shown in Figure 7. With the length of tailgroups increasing, the density profiles can extend to a greater range along the *z*-axis, corresponding to a swelling supramolecular structure. Similar behavior has been observed in Figure 8 for the effect of the headgroup length. Longer headgroups produce better coverage over the graphene surface. However, in the case of C12E3, C12E5, and C12E10 surfactants on the graphene sheet, there is no formation of hemispheres; instead, only hemicylindrical micelles with different radius appear. This is due to the situation that it is unlikely to form hemisphere structures with longer tailgroups. As expected, the radius of the hemicylinders increases as the headgroups become elongated. As observed in Figure 8, long PEO segments usually provide larger steric repellence in preventing possible aggregation between graphene sheets, therefore providing better dispersion for graphene nanoparticles in solution.[26,57]

3.5. Effect of the Width of Graphene Sheets. We also investigated the self-assembly structures and morphologies for the nonionic surfactants adsorbed on graphene nanoribbons (GNRs)[58] with different widths. Figure 9 shows the representative structures for the C12E5 surfactants adsorbed on the 20 nm long GNRs with the widths of 2.0, 4.0, and 6.0 nm, respectively. In these simulations, the same adsorption area of 0.53 nm^2/molecule was considered.

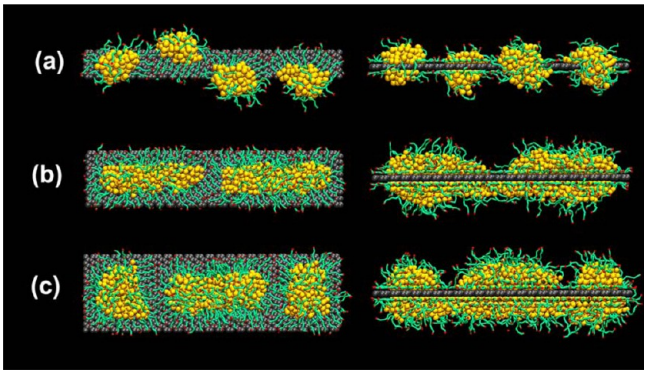

Figure 9. Snapshots of equilibrium morphologies of C12E5 surfactants on 20 nm long GNR with three widths of (a) 2.0, (b) 4.0, and (c) 6.0 nm. Notice the two views for each system: left is a front view; right is a side view. Water molecules are removed for clarity; color scheme and other details are the same as that in Figure 4.

In the case of 2.0 nm GNR, the length of the C12E5 surfactant is usually larger than the GNR width. It can be

dx.doi.org/10.1021/jp3043939 | J. Phys. Chem. B 2012, 116, 12048−12056

observed that self-assembly morphology of C12E5 on the 2.0 nm GNR surface shows several scattered hemispheric micelles wrapping the GNR. We can conclude that the narrow GNR promotes the formation of hemisphere structures on the nanosized surface. Because of an excluded-volume effect between headgroups, some hemispherical micelles wrap up the side edge of GNR. This aggregate structure is different from the morphology[35] for SDS adsorbed on the narrow GNR surface (2.0 nm in width) in which SDS surfactants are completely oriented along the width direction of GNR. This discrepancy is likely caused by the extending headgroups in the alkyl PEO surfactants.[50]

On the wider GNR (4.0 nm) that is close to twice the length of the C12E5 surfactant (~2.3 nm), we observed that C12E5 surfactants aggregate to form hemicylinders orienting along the longitudinal axis of the GNR. In this way, the headgroups can, to larger extent, protrude into the aqueous phase while keeping most of the tailgroups and graphene surface isolated away from water. It was noted that the self-assembly structure on the top surface of the GNR is somewhat different from that observed on the bottom. On the GNR with 6.0 nm width that exceeds twice the surfactant length, the surfactants yield hemispheres on the two ends of the graphene sheet and forms a hemicylinder in the middle region on the top surface. These diverse morphologies or structures are not consistent with those observed on macroscopic graphite surfaces possibly due to nanoscale effect. Our simulation provides direct evidence that the size effect of graphene is able to assist in achieving controllable regular pattern of aggregate structures on a nanoscale surface, which might act as grafting sites in the construction of nanohybrids.

4. CONCLUSIONS

In this study, the adsorption and self-assembly of the alkyl-PEO surfactants on a nanosized graphene surfaces have been simulated by means of CG molecular dynamics simulation. The Martini force field was used, which can well reproduce the experimental result of the self-assembly structures and morphologies of nonionic surfactants in bulk aqueous solution and on the graphite surface. This CG simulation allows us to probe complicated self-assembly behavior on graphene with larger time- and length-scales. The dynamic adsorption process was clarified. Two adsorption modes on nanoscale graphene, including surface adsorption and side edge adsorption, have been observed.

The supramolecular self-assembly structures and morphologies of the nonionic surfactants on graphene nanostructures were probed under different concentrations. At low concentration, the surfactants involve a parallel arrangement with a monolayer structure. With concentration increasing, various morphological hemimicelles, including hemispheres, hemicylinders, and U-shaped hemimicelles, can form, respectively. Meanwhile, our CG simulation also shows the effect of the length of tailgroup and headgroup segments on the supramolecular nanostructures. The surfactants with a short tail yield hemisphere adsorption. For a longer tail structure, the surfactants assemble into the hemicylindrical micelles. The radius of the hemicylinders increases as the surfactant becomes elongated, leading to a larger spatial volume of the supramolecular structures. We also demonstrated the representative structural features for the surfactants adsorbed on the GNRs with varying widths. The surfactants on narrow GNR can spontaneously assemble into spherical micelles wrapping up the side edge of GNR. For wider GNR, hemicylinders are formed. However, for the width of GNR that exceeds twice the length of the surfactant, hemispheres emerge at both ends of GNR. In summary, our simulation provides comprehensive insights into the supramolecular self-assembly structures of nonionic surfactants on nanoscale graphene.

■ ASSOCIATED CONTENT

Supporting Information

Detailed systems of CG molecular dynamics simulations; the snapshots of C12E5 aggregated on graphene at the oversaturated surface coverage; the dynamic processes of 300 C12E5 self-assembly on another graphene nanosheet; and the movie related to the self-assembly process of the C12E5 surfactants on graphene. This material is available free of charge via the Internet at http://pubs.acs.org.

■ AUTHOR INFORMATION

Corresponding Author

*Tel: 86-025-83587184. Fax: 86-025-83587184. E-mail: Yangxia@njut.edu.cn.

Notes

The authors declare no competing financial interest.

■ ACKNOWLEDGMENTS

This work was supported by the National Natural Science Foundation of China under Grants 21176114 and 20976079, the Jiangsu Qinglan Project, and the State Key Laboratory of Materials-Oriented Chemical Engineering.

■ REFERENCES

(1) Geim, A. K.; Novoselov, K. S. *Nat. Mater.* **2007**, *6*, 183−191.
(2) Novoselov, K. S.; Geim, A. K.; Morozov, S. V.; Jiang, D.; Zhang, Y.; Dubonos, S. V.; Grigorieva, I. V.; Firsov, A. A. *Science* **2004**, *306*, 666−669.
(3) Geim, A. K. *Science* **2009**, *324*, 1530−1534.
(4) Stankovich, S.; Dikin, D. A.; Dommett, G. H. B.; Kohlhaas, K. M.; Zimney, E. J.; Stach, E. A.; Piner, R. D.; Nguyen, S. T.; Ruoff, R. S. *Nature* **2006**, *442*, 282−286.
(5) Paek, S. M.; Yoo, E.; Honma, I. *Nano Lett.* **2009**, 72−75.
(6) Wang, X. R.; Tabakman, S. M.; Dai, H. J. *J. Am. Chem. Soc.* **2008**, *130*, 8152−8153.
(7) Qu, L. T.; Liu, Y.; Baek, J. B.; Dai, L. M. *ACS Nano* **2010**, *4*, 1321−1326.
(8) Yang, P. D.; Zhao, D. Y.; Margolese, D. I.; Chmelka, B. F.; Stucky, G. D. *Nature* **1998**, *396*, 152−155.
(9) Zhao, D. Y.; Feng, J. L.; Huo, Q. S.; Melosh, N.; Fredrickson, G. H.; Chmelka, B. F.; Stucky, G. D. *Science* **1998**, *279*, 548−552.
(10) Meng, Y.; Gu, D.; Zhang, F. Q.; Shi, Y. F.; Yang, H. F.; Li, Z.; Yu, C. Z.; Tu, B.; Zhao, D. Y. *Angew. Chem.* **2005**, *44*, 7053−7059.
(11) Braun, P. V.; Osenar, P.; Stupp, S. I. *Nature* **1996**, *380*, 325−328.
(12) Wang, D. H.; Choi, D. W.; Li, J.; Yang, Z. G.; Nie, Z. M.; Kou, R.; Hu, D. H.; Wang, C. M.; Saraf, L. V.; Zhang, J. G.; Aksay, I. A.; Liu, J. *ACS Nano* **2009**, *3*, 907−914.
(13) Wang, D. H.; Kou, R.; Choi, D. W.; Yang, Z. G.; Nie, Z. M.; Li, J.; Saraf, L. V.; Hu, D. H.; Zhang, J. G.; Graff, G. L.; Liu, J.; Pope, M. A.; Aksay, I. A. *ACS Nano* **2010**, *4*, 1587−1595.
(14) Wang, Z. M.; Wang, W. D.; Coombs, N.; Soheilnia, N.; Ozin, G. A. *ACS Nano* **2010**, *4*, 7437−7450.
(15) Korkut, S.; Roy-Mayhew, J. D.; Dabbs, D. M.; Milius, D. L.; Aksay, I. A. *ACS Nano* **2011**, *5*, 5214−5222.
(16) Coleman, J. N. *Adv. Funct. Mater.* **2009**, *19*, 3680−3695.
(17) Lotya, M.; Hernandez, Y.; King, P. J.; Smith, R. J.; Nicolosi, V.; Karlsson, L. S.; Blighe, F. M.; De, S.; Wang, Z. M.; McGovern, I. T.;

Duesberg, G. S.; Coleman, J. N. *J. Am. Chem. Soc.* **2009**, *131*, 3611−3620.
(18) Lotya, M.; King, P. J.; Khan, U.; De, S.; Coleman, J. N. *ACS Nano* **2010**, *4*, 3155−3162.
(19) Green, A. A.; Hersam, M. C. *Nano Lett.* **2009**, *9*, 4031−4036.
(20) Sánchez-Ferrer, A.; Bru, R.; García-Carmona, F. *Crit. Rev. Biochem. Mol. Biol.* **1994**, *29*, 275−313.
(21) Fu, Y. J.; Nitecki, D. E.; Maltby, D.; Simon, G. H.; Berejnoi, K.; Raatschen, H. J.; Yeh, B. M.; Shames, D. M.; Brasch, R. C. *Bioconjugate Chem.* **2006**, *17*, 1043−1056.
(22) Lin, Y.; Allard, L. F.; Sun, Y. P. *J. Phys. Chem. B* **2004**, *108*, 3760−3764.
(23) Zheng, X. I.; Xu, Q.; He, L. H.; Yu, N.; Wang, S. S.; Chen, Z. M.; Fu, J. W. *J. Phys. Chem. B* **2011**, *115*, 5815−5826.
(24) Li, B.; Li, L. Y.; Wang, B. B.; Li, C. Y. *Nat. Nanotechnol.* **2009**, *4*, 358−362.
(25) Zu, S. Z.; Han, B. H. *J. Phys. Chem. C* **2009**, *113*, 13651−13657.
(26) Seo, J. W. T.; Green, A. A.; Antaris, A. L.; Hersam, M. C. *J. Phys. Chem. Lett.* **2011**, *2*, 1004−1008.
(27) Carswell, A. D. W.; O'Rear, E. A.; Grady, B. P. *J. Am. Chem. Soc.* **2003**, *125*, 14793−14800.
(28) Patrick, H. N.; Warr, G. G.; Manne, S.; Aksay, I. A. *Langmuir* **1997**, *13*, 4349−4356.
(29) Chun, J.; Li, J. L.; Car, R.; Aksay, I. A.; Saville, D. A. *J. Phys. Chem. B* **2006**, *110*, 16624−16632.
(30) Atkin, R.; Warr, G. G. *J. Am. Chem. Soc.* **2005**, *127*, 11940−11941.
(31) Schniepp, H. C.; Saville, D. A.; Aksay, I. A. *J. Am. Chem. Soc.* **2006**, *128*, 12378−12379.
(32) Patrick, H. N.; Warr, G. G. *Colloids Surf., A* **2000**, *162*, 149−157.
(33) Schatz, G. C. *Proc. Natl. Acad. Sci. U.S.A.* **2007**, *104*, 6885−6892.
(34) Xu, Z. J.; Yang, X. N.; Yang, Z. *Nano Lett.* **2010**, *10*, 985−991.
(35) Tummala, N. R.; Grady, B. P.; Striolo, A. *Phys. Chem. Chem. Phys.* **2010**, *12*, 13137−13143.
(36) Lin, S. C.; Shih, C. J.; Strano, M. S.; Blankschtein, D. *J. Am. Chem. Soc.* **2011**, *133*, 12810−12823.
(37) Srinivas, G.; Nielsen, S. O.; Moore, P. B.; Klein, M. L. *J. Am. Chem. Soc.* **2006**, *128*, 848−853.
(38) Marrink, S. J.; de Vries, A. H.; Mark, A. E. *J. Phys. Chem. B* **2004**, *108*, 750−760.
(39) Wallace, E. J.; Sansom, M. S. P. *Nano Lett.* **2007**, *7*, 1923−1928.
(40) Marrink, S. J.; Risselada, H. J.; Yefimov, S.; Tieleman, D. P.; de Vries, A. H. *J. Phys. Chem. B* **2007**, *111*, 7812−7824.
(41) Titov, A. V.; Král, P.; Pearson, R. *ACS Nano* **2010**, *4*, 229−234.
(42) Plimpton, S. *J. Comput. Phys.* **1995**, *117*, 1−19.
(43) Lee, H.; de Vries, A. H.; Marrink, S. J.; Pastor, R. W. *J. Phys. Chem. B* **2009**, *113*, 13186−13194.
(44) Wallace, E. J.; Sansom, M. S. P. *Nanotechnology* **2009**, *20*, 045101.
(45) Wallace, E. J.; Sansom, M. S. P. *Nano Lett.* **2008**, *8*, 2751−2756.
(46) Funari, S. S.; Rapp, G. *J. Phys. Chem. B* **1997**, *101*, 732−739.
(47) Shinoda, W.; Devane, R.; Klein, M. L. *Mol. Simul.* **2007**, *33*, 27−36.
(48) Holmberg, K.; Jönsson, B.; Kronberg, B.; Lindman, B. *Surfactants and Polymers in Aqueous Solution*; John Wiley & Sons, Ltd.: West Sussex, U.K., 2002.
(49) Sammalkorpi, M.; Panagiotopoulos, A. Z.; Haataja, M. *J. Phys. Chem. B* **2008**, *112*, 12954−12961.
(50) Bedrov, D.; Smith, G. D. *Langmuir* **2006**, *22*, 6189−6194.
(51) Kjellin, U. R. M.; Claesson, P. M.; Linse, P. *Langmuir* **2002**, *18*, 6745−6753.
(52) Poulin, P.; Vigolo, B.; Launois, P. *Carbon* **2002**, *40*, 1741−1749.
(53) Sammalkorpi, M.; Panagiotopoulos, A. Z.; Haataja, M. *J. Phys. Chem. B* **2008**, *112*, 2915−2921.
(54) Schniepp, H. C.; Shum, H. C.; Saville, D. A.; Aksay, I. A. *J. Phys. Chem. B* **2008**, *112*, 14902−14906.
(55) Calvaresi, M.; Dallavalle, M.; Zerbetto, F. *Small* **2009**, *5*, 2191−2198.
(56) Holland, N. B.; Ruegsegger, M.; Marchant, R. E. *Langmuir* **1998**, *14*, 2790−2795.
(57) Moore, V. C.; Strano, M. S.; Haroz, E. H.; Hauge, R. H.; Smalley, R. E. *Nano Lett.* **2003**, *3*, 1379−1382.
(58) Cai, J. M.; Ruffieux, P.; Jaafar, R.; Bieri, M.; Braun, T.; Blankenburg, S.; Muoth, M.; Seitsonen, A. P.; Saleh, M.; Feng, X. L.; Mullen, K.; Fasel, R. *Nature* **2010**, *466*, 470−473.